Analysing radiative and non-radiative recombination in InAs QDs on Si for integrated laser applications

Jonathan R. Orchard[1], Chris Woodhead[2], Samuel Shutts[3], Jiang Wu[4], Angela Sobiesierski[3], Rob J. Young[2], Richard Beanland[5], Huiyun Liu[4], Peter M. Smowton[4], David J. Mowbray[1]
[1]Department of Physics, University of Sheffield, Hicks Building, Hounsfield Road, Sheffield, S3 7RH
[2]Department of Physics, University of Lancaster, Lancaster, LA1 4YB
[3]School of Physics and Astronomy, Cardiff University, Queen's Buildings, The Parade, Cardiff, CF24 3AA
[4]Department of Electronic & Electrical Engineering, University College London, Torrington Place, London, WC1E 7JE
[5]Department of Physics, University of Warwick, Coventry, CV4 7AL

ABSTRACT

Three InAs quantum dot (QD) samples with dislocation filter layers (DFLs) are grown on Si substrates with and without in-situ annealing. Comparison is made to a similar structure grown on a GaAs substrate. The three Si grown samples have different dislocation densities in their active region as revealed by structural studies. By determining the integrated emission as a function of laser power it is possible to determine the power dependence of the radiative efficiency and compare this across the four samples. The radiative efficiency increases with decreasing dislocation density; this also results in a decrease in the temperature quenching of the PL. A laser structures grown on Si and implementing the same optimum DFL and annealing procedure exhibits a greater than 3 fold reduction in threshold current as well as a two fold increase in slope efficiency in comparison to a device in which no annealing is applied.

Keywords: Quantum dots, dislocation filter layers, semiconductor lasers, silicon photonics

1. INTRODUCTION

As silicon continues to expand as a platform for photonic components, the need increases for an efficient, electrically driven laser grown directly on a silicon substrate [1]. This requires a novel approach due to the indirect bandgap of Si. Many approaches have been investigated; including rare earth doped Si, stimulated Raman scattering, nanostructure Si and heterogeneous/monolithic integration of III-V and Si [2-6]. Several successful demonstrations of room temperature lasing have been reported including Si Raman lasers, hybrid Si lasers and III-V and Ge lasers grown on Si [3,4]. However, each of these methods still requires significant development in order to provide a manufacturable solution. Ge-on-Si lasers need to overcome high optical losses and demonstrate the high optical gains required for electrically pumped lasers [5], while devices such as Raman lasers are limited so far to optically pumped operation [6].

Of the approaches listed above, heterogeneous/monolithic integration of III-V and Si yields the most promising results, with wafer bonded devices demonstrating milliwatt output power and continuous wave operation to above 100 °C [7,8]. However, the yield and reliability of these devices has yet to be demonstrated [9,10]. Direct growth of III-V materials onto Si substrates is considered the most manufacturable approach, but the high dislocation densities that arise from the GaAs-Si lattice mismatch and their different thermal expansion coefficients present challenges [11,12]. The use of quantum dots (QDs) as the gain media in these devices has been proposed as they have a reduced sensitivity to defects compared with quantum wells (QWs). This is a result of their localisation of carriers, which reduces migration to non-radiative centres associated with dislocations. In addition, QDs have the potential of reduced temperature sensitivity when used as the laser gain medium. To date, several reports have been published demonstrating high output powers and high temperature operation from III-V QD lasers grown directly on Si substrates [13-19].

Although QDs are significantly less sensitive to dislocations than QWs, laser performance (e.g. threshold current, operating lifetime etc.) is expected to benefit from a reduction in the dislocation density present in the active region. This can be achieved by careful design of the layers above the III-V/Si interface; previously we have described a method using in-situ annealing and strained super lattice layers, referred to as dislocation filter layers (DFLs), to reduce the dislocation density reaching the active region [20]. In designing these structures there is a trade off between the number of layers used to reduce dislocation propagation and multiplication and minimizing the total structure thickness. Due to the difference in thermal expansion coefficients between the Si and III-V materials there is a critical thickness above which cracking of the III-V material will occur. In this paper we compare samples with varying dislocation densities present in the III-V QD active region against a reference sample grown on a GaAs substrate. We analyse the effect of dislocation density on the radiative and non-radiative efficiency, as well as temperature dependent performance. Finally, we examine laser structures containing the same dislocation reducing layers and study the effect on laser performance.

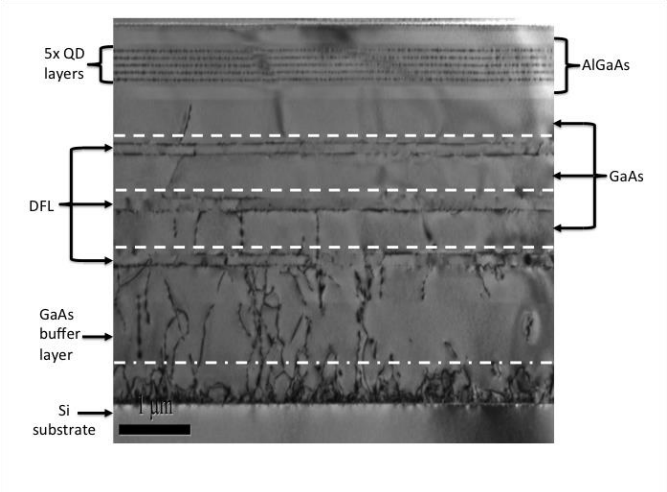

Figure 1. TEM image of a dislocation filter layer sample, the dashed lines indicate where annealing steps were carried out.

2. EPITAXIAL GROWTH AND DEFECT ANALYSIS

The typical DFL sample structure is shown in the TEM image of *Figure 1.* InAs/GaAs QD structures were grown on n-doped Si (100) substrates with 4° offcut to the [011] plane using a solid-source III-V molecular beam epitaxy system (MBE). Oxide desorption of the Si substrates was performed at 900 °C for 10 minutes. The substrates were then cooled down to 400 °C for the growth of a GaAs nucleation layer, comprising an optimized two-step growth scheme [3,14]. Three repeats of the DFLs separated by 400-nm GaAs spacer layers were grown after a 1000-nm GaAs buffer layer (5 DFLs were used in the laser structure). The DFLs consisted of five-periods of 10-nm $In_{0.18}Ga_{0.82}As$/10-nm GaAs. After the DFLs a 400-nm GaAs spacer layer was deposited followed by an InAs/GaAs dot-in-a-well (DWELL) structure grown at ~510 °C, similar to that optimized on GaAs substrates [21-23]. The 5 DWELLs were embedded between two 100-nm GaAs layers grown at 580 °C and 50-nm AlGaAs layers grown at 610 °C. Each DWELL consisted of a 3-monolayer InAs QD layer sandwiched between 2 and 6-nm $In_{0.15}Ga_{0.85}As$ layers. A 45 nm undoped GaAs spacer layer separated the InAs/InGaAs DWELLs.

Table 1. List of annealing steps applied to each sample and the resulting dislocation reduction measured at the active region relative to the Si-III/V interface.

Sample	Anneal steps	Dislocation reduction
A	None	95.6%
B	1 step	98.9%
C	2 step	99.9%
Control	N/A	N/A

The annealing schemes used to enhance the effect of the DFLs are summarised in *Table 1*. No annealing was applied to sample A. Sample B was annealed at 600 °C after the growth of the GaAs buffer layer, denoted by the dashed lines in

Figure 1. Sample C was annealed at 600 °C at the dashed lines and at 600 °C at the dot-dash lines. All annealing was carried out during growth in the MBE reactor. The control sample was grown on a GaAs substrate with a thinner GaAs buffer layer of 200 nm grown at 580 °C and no DFLs, but with the same 5 layer QD DWELL active region. In the laser structures the AlGaAs thickness was increased to 1200 nm and 2×10^{18} cm^{-3} n dopant was added to the lower cladding and 2×10^{18} cm^{-3} p dopant was added to the upper cladding, with 1×10^{19} cm^{-3} p dopant in the capping layer.

In order to quantify the effect of the annealing on the defect propagation TEM images, similar to *Figure 1* but for a much greater area, were recorded for each sample. Cross-section TEM specimens parallel to {110} were prepared using standard protocols, each of which typically yielded 30–60 μm of electron transparent area along the Si/III-V interface. A series of images were taken using bright field g 220 diffraction conditions with the specimen tilted 5°–10° from the {110} zone axis, capturing the complete structure as shown in *Figure 1* over the entire electron transparent area (see [24] for further details). From these images it is possible to accurately determine the number of defects present at different levels in the structure, thereby quantifying the efficacy of the DFLs and annealing process. In sample A, where no annealing was applied, the defect reduction in the active region relative to the initial number at the Si-GaAs interface was 95.6%. The addition of annealing in sample B increased this reduction to 98.9% and for sample C, where a further annealing step was added, the reduction was 99.9%. These results clearly demonstrate the benefits of including the in-situ annealing during the growth of the structures.

3. RESULTS AND DISCUSSION

In order to analyse the effect of the reduction in dislocation density on the sample optical quality, power dependent photoluminescence (PL) was measured. Each sample was excited by a 1064 nm laser, with a 100 μm focused spot, over a range of powers between 1 (10 Wcm^{-2}) and 125 mW (1600 Wcm^{-2}), the luminescence produced by each sample was dispersed in a 0.75 m spectrometer and detected using a liquid nitrogen cooled Ge detector. Excitation was carried out at 1064 nm to ensure carriers were generated only within the QD layers, allowing processes only occurring in the active layers to be studied. *Figure 2* shows the PL spectra for each of the samples for 50 mW of excitation power at 300 K. The control sample has the brightest intensity, a consequence of the lower dislocation density due to the all III-V structure. Additionally, the control sample has a longer emission wavelength than the samples grown on Si substrates, this is due to a small degree of strain in the samples grown on Si substrates which results from the different thermal expansion coefficients of the Si and III-V materials [20]. Sample A has the lowest intensity PL, which correlates with having the highest dislocation density. Samples B and C, where annealing steps were included, have very similar peak luminescence intensities (within ~5%), but sample C has a greater integrated luminescence intensity (10% larger), again matching well with their respective dislocation densities. Although the active region growth is identical for each sample, sample C has a much broader ground state linewidth (57 nm) compared with either sample B (38 nm) or the control (42 nm), it is believed that this sample has a larger subset of smaller QDs compared to the other samples. No excited state emission is seen in any of the samples as only a very small percentage ($5x10^{-4}$ %) of the exciting photons are absorbed by the QD layers.

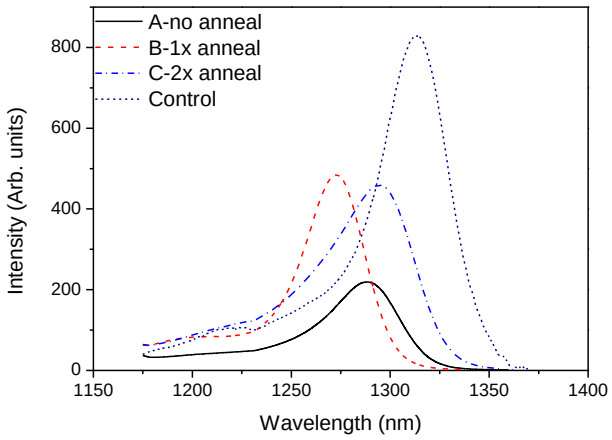

Figure 2. Room temperature photoluminescence spectra for samples excited with 50 mW at 1064 nm

Obtaining the integrated PL intensity for each of the samples as a function of excitation power allows radiative and non-radiative parameters to be obtained by fitting the data with equation 1 as outlined in [25].

$$P_{laser} = P_1\sqrt{I_{PL}} + P_2 I_{PL} + P_3 I_{PL}^{3/2} \quad (1)$$

The coefficients P_1, P_2, P_3 are analogous to the standard A, B, C coefficients and refer to the defect-related recombination, radiative recombination and Auger recombination respectively. From the fitting data it is possible to calculate the radiative efficiency (η) as a function of laser power, this is plotted in *Figure 3*. Due to the low QD carrier occupancy the P_3 term is ignored as this is related to the Auger effect, which is a 3-carrier process. For all samples the radiative efficiency increases with increasing power as defects become saturated. At the highest laser power the control sample exhibits the highest radiative efficiency (88 %), followed by sample B (73 %), then sample C (64 %) and sample A (62 %). The result for sample C is surprising as this has the lowest defect density of all the samples grown on Si; a radiative efficiency greater than or equal to sample B would be expected. The cause of this lower efficiency may be related to the larger linewidth of the emission which results in a larger fraction of QDs having a smaller size and as a consequence a shorter wavelength emission and hence lower carrier confinement. This can result in increased thermal carrier loss from these smaller QDs. In addition the smaller QDs could also have a reduced oscillator strength due to a greater leakage of the electron wave function out of the dots. However these results show that including at least one annealing step improves the radiative efficiency of the structure although this efficiency remains lower than that of reference structure grown on GaAs.

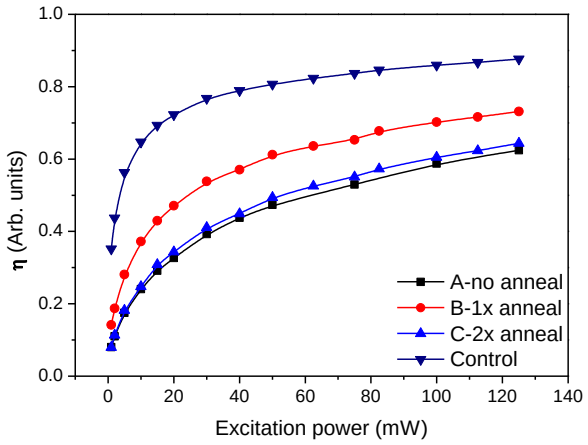

Figure 3. Room temperature radiative efficiency of the different samples for a range of excitation powers

An alternative method to assess the effect of dislocations on the material quality is to study the PL quenching with temperature. The integrated spectral intensities for the different samples were determined at a fixed excitation power of 10 mW using a 638 nm laser, over the temperature range 77 to 300K. Intensities were normalised to the intensity at 77 K and log intensity plotted as a function of temperature, shown in *Figure 4*. Sample A exhibits the largest drop off in intensity; followed by sample B, sample C and finally the control sample. This quenching behaviour is attributed to the thermal escape of carriers from the QD ground state into the continuum followed by non-radiative recombination in the barriers [23,26]. This is consistent with a carrier loss process that occurs following carrier capture by the QDs. Replotting the data in *Figure 4* against 1/T allows the thermal activation energy, E_a, to be determined for each of the samples, giving energies of 130±10 meV, 120±10 meV, 140±10 meV and 140±10 meV for samples A, B, C and control respectively. The variation of the activation energies correlates well with the variation in emission wavelength, for example a larger confinement potential in the longer wavelength samples (C and control). The reduction in PL quenching with increased number of annealing steps is a clear indicator of the benefit of annealing on reducing the dislocation density and that two annealing steps are more beneficial than one. For devices operating around room temperature the radiative efficiency of the sample with two annealing steps varies less rapidly than that of samples with one or no annealing steps.

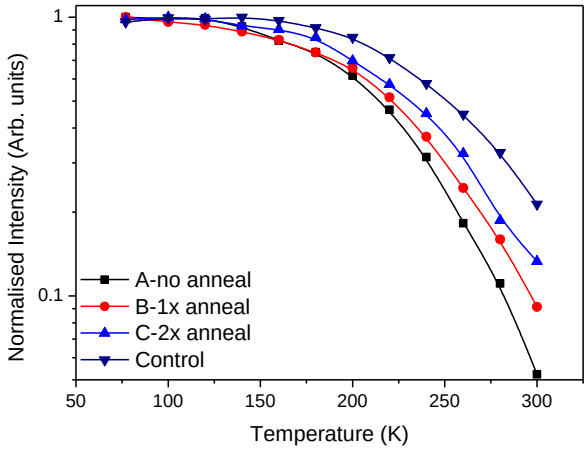

Figure 4. Normalised integrated PL intensity as a function of temperature for each of the samples at an excitation power of 10mW

In order to further assess the relative advantages of the annealing steps, full laser structures with thicker and doped cladding layers were grown. The wafers were processed into 10 µm ridge lasers, with the waveguide dry-etched down to the lower n-doped layer to allow the formation of an AuGe/Ni/Au contact. Facets were also dry-etched to circumvent the difficulty of forming cleaved-facets on the Si substrates. Benzocyclobutene (BCB) was used to planarise the samples and Cr-Au was deposited for the p-contact. Lasers were driven pulsed, with a repetition rate of 1 kHz and a pulse width of 1 µs to prevent self-heating effects. The current versus emitted power characteristics for 3 mm long lasers processed from each wafer are shown in *Figure 5*. Sample A had the highest threshold current of 382 mA, followed by sample B with 287 mA and then sample C with 103 mA. Measuring the external differential quantum efficiency, η_d, for each sample gives values of 35, 53 and 90 % for samples A, B and C respectively. The number of dislocations can affect laser performance in two main ways, acting as non-radiative recombination centres to increase threshold current or contributing to internal loss (α_i) by scattering photons out of the lasing mode. These combine to both reduce the slope efficiency and increase the threshold current. The latter occurs both because more carriers are lost to non-radiative recombination and also increased gain is required to overcome the increased internal loss. The increase in gain is reflected in the lasing wavelengths of the samples, with samples A and B lasing from an excited state at 1211 and 1228 nm respectively, where the available gain is higher due to increased degeneracy. Sample C has an emission wavelength of 1286 nm indicating the internal loss is low enough to achieve lasing from the ground state. The reduction in threshold current and increase in slope efficiency with increased number of annealing steps correlates with the reduction in dislocation density and that devices with two steps have significantly better characteristics than those with one or no steps. This also highlights the anomalous behaviour of the annealed PL structure with two annealing steps, which we attribute to an issue during growth that resulted in an increased number of smaller QDs in the distribution.

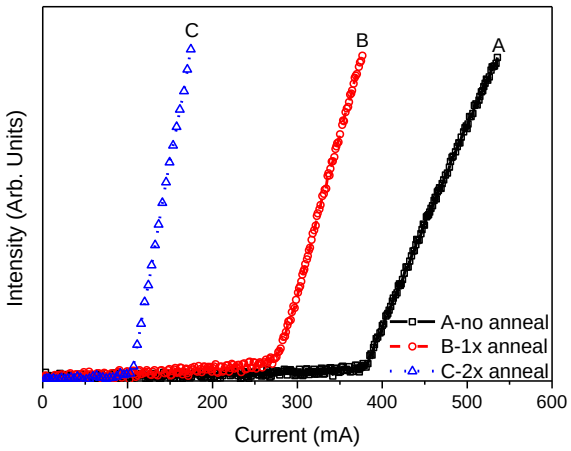

Figure 5. Pulsed current vs. single facet power characteristic for the 3 samples on Si substrates at room temperature

4. CONCLUSION

We have described an optical and structural study of InAs QD structures grown directly on Si substrates. Samples differ in the number of annealing steps which are applied to increase the efficiency of the defect filter layers grown between the Si / III-V interface and QD active region. Comparison is made to a very similar structure grown on GaAs. Samples with lower dislocation densities in the active region exhibit increased radiative efficiency and reduced PL quenching with increasing temperature. Comparing laser devices with the same DFLs and non or two annealing steps shows a greater than three-fold reduction in threshold current density and a greater than two-fold increase in slope efficiency. This indicates that dislocations, which remain in the active region affect both the radiative efficiency and internal loss. Radiative efficiencies of the best Si grown samples are still below that of the full III-V structure, indicating that further improvements of the dislocation reduction are desirable.

REFERENCES

[1] B. Jalali and S. Fathpour, "Silicon photonics," J. Lightwave Technol. **24**(12), 4600–4615 (2006).

[2] J. Liu, X. Sun, R. Camacho-Aguilera, L. C. Kimerling, and J. Michel, "Ge-on-Si laser operating at room temperature," Opt. Lett. **35**(5), 679–681 (2010).

[3] T. Wang, H. Liu, A. Lee, F. Pozzi, and A. Seeds, "1.3-μm InAs/GaAs quantum-dot lasers monolithically grown on Si substrates," Opt. Express **19**(12), 11381–11386 (2011).

[4] Z. Yuan, A. Anopchenko, N. Daldosso, R. Guider, D. Navarro-Urrios, A. Pitanti, R. Spano, and L. Pavesi, "Silicon nanocrystals as an enabling material for silicon photonics," Proc. IEEE **97**(7), 1250–1268 (2009).

[5] X. Chen, C. Li, and H. K. Tsang, "Device engineering for silicon photonics," NPG Asia Materials **3**(1), 34–40 (2011).

[6] R. E. Camacho-Aguilera, Y. Cai, N. Patel, J. T. Bessette, M. Romagnoli, L. C. Kimerling, and J. Michel, "An electrically pumped germanium laser," Opt. Express **20**(10), 11316–11320 (2012).

[7] S. Tanaka, S. H. Jeong, S. Sekiguchi, T. Kurahashi, Y. Tanaka, and K. Morito, "High-output-power, single-wavelength silicon hybrid laser using precise flip-chip bonding technology," Opt. Express **20**(27), 28057–28069 (2012).

[8] H. H. Chang, A. W. Fang, M. N. Sysak, H. Park, R. Jones, O. Cohen, O. Raday, M. J. Paniccia, and J. E. Bowers, "1310nm silicon evanescent laser," Opt. Express **15**(18), 11466–11471 (2007).

[9] K. Tanabe, D. Guimard, D. Bordel, S. Iwamoto, and Y. Arakawa, "Electrically pumped 1.3 microm room-temperature InAs/GaAs quantum dot lasers on Si substrates by metal-mediated wafer bonding and layer transfer," Opt. Express **18**(10), 10604–10608 (2010).

[10] R. Chen, T. D. Tran, K. W. Ng, W. S. Ko, L. C. Chuang, F. G. Sedgwick, and C. Chang-Hasnain, "Nanolasers grown on silicon," Nat. Photonics **5**(3), 170–175 (2011).

[11] K. Tanabe, K. Watanabe, and Y. Arakawa, "III-V/Si hybrid photonic devices by direct fusion bonding," Sci Rep **2**, 349 (2012).

[12] D. Liang and J. E. Bowers, "Recent progress in lasers on silicon," Nat. Photonics **4**(8), 511–517 (2010).

[13] H. Liu, "III–V Quantum-Dot Materials and Devices Monolithically Grown on Si Substrates," in *Silicon-based Nanomaterials*, H. Li, J. Wu, and Z. M. Wang, eds. (Springer New York, 2013), pp. 357–380.

[14] H. Liu, T. Wang, Q. Jiang, R. Hogg, F. Tutu, F. Pozzi, and A. Seeds, "Long-wavelength InAs/GaAs quantum-dot laser diode monolithically grown on Ge substrate," Nat. Photonics **5**(7), 416–419 (2011).

[15] A. D. Lee, Q. Jiang, M. Tang, Y. Zhang, A. J. Seeds, and H. Liu, "InAs/GaAs quantum-dot lasers monolithically grown on si, ge, and ge-on-si substrates," IEEE J. Sel. Top. Quantum Electron. **19**(4), 1901107 (2013).

[16] A. Lee, Q. Jiang, M. Tang, A. Seeds, and H. Liu, "Continuous-wave InAs/GaAs quantum-dot laser diodes monolithically grown on Si substrate with low threshold current densities," Opt. Express **20**(20), 22181–22187 (2012).

[17] T. Wang, A. Lee, F. Tutu, A. Seeds, H. Liu, Q. Jiang, K. Groom, and R. Hogg, "The effect of growth temperature of GaAs nucleation layer on InAs/GaAs quantum dots monolithically grown on Ge substrates," Appl. Phys. Lett. **100**(5), 052113 (2012).

[18] A. Y. Liu, C. Zhang, J. Norman, A. Snyder, D. Lubyshev, J. M. Fastenau, A. W. Liu, A. C. Gossard, and J. E. Bowers, "High performance continuous wave 1.3 μm quantum dot lasers on silicon," Appl. Phys. Lett. **104**(4), 041104 (2014).

[19] A. Y. Liu, C. Zhang, A. Snyder, D. Lubyshev, J. M. Fastenau, A. W. Liu, A. C. Gossard, and J. E. Bowers, "MBE growth of P-doped 1.3 μm InAs quantum dot lasers on silicon," J. Vac. Sci. Technol. B **32**, 02C108 (2014).

[20] J. R. Orchard, J. Wu, S. Chen, Q. Jiang, T. Ward, R. Beanland, H. Liu, D. J. Mowbray, "Optimising the defect filter layer design III/V QDs on Si for integrated laser applications," Proc. SPIE 9373, 93730G (2015).

[21] H. Liu, M. Hopkinson, C. Harrison, M. Steer, R. Frith, I. Sellers, D. Mowbray, and M. Skolnick, "Optimizing the growth of 1.3 μm InAs/InGaAs dots-in-a-well structure," J. Appl. Phys. **93**(5), 2931–2936 (2003).
[22] H. Liu, D. Childs, T. Badcock, K. Groom, I. Sellers, M. Hopkinson, R. Hogg, D. Robbins, D. Mowbray, and M. Skolnick, "High-performance three-layer 1.3-μm InAs-GaAs quantum-dot lasers with very low continuous-wave room-temperature threshold currents," IEEE Photon. Technol. Lett. **17**(6), 1139–1141 (2005).
[23] H. Liu, I. Sellers, T. Badcock, D. Mowbray, M. Skolnick, K. Groom, M. Gutierrez, M. Hopkinson, J. Ng, J. David, and R. Beanland, "Improved performance of 1.3 μm multilayer InAs quantum-dot lasers using a high-growth-temperature GaAs spacer layer," Appl. Phys. Lett. **85**(5), 704–706 (2004).
[24] I. George, F. Becagli, H.-Y Liu, J. Wu, M. Tang and R. Beanland, "Dislocation filters in GaAs on Si," Semicond. Sci. Tech. **30**(11) (2015).
[25] Y. S. Yoo, T. M. Roh, J. H. Na, S. J. Son, Y. H. Cho, "Simple analysis method for determining internal quantum efficiency and relative recombination ratios in light emitting diodes," Appl. Phys. Lett. **102**, 211107 (2013).
[26] R. Chen, H. Liu, and H. Sun, "Electronic energy levels and carrier dynamics in InAs/InGaAs dots-in-a-well structure investigated by optical spectroscopy," J. Appl. Phys. **107**(1), 013513 (2010).